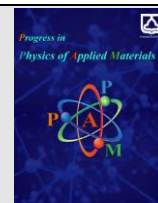




Semnan University

journal homepage: <https://ppam.semnan.ac.ir/>

Electronic and spintronic transport in gapped graphene-based FG/SG/FG junctions

H. Karbaschi^{a*}, G. Rashedi^b^a Faculty of science, Mahallat Institute of Higher Education, Mahallat 37811-51958, Iran^b Department of Physics, University of Isfahan, Isfahan 81746-73441, Iran

ARTICLE INFO

Article history:

Received: 12 May 2024

Revised: 11 June 2024

Accepted: 24 June 2024

Keywords:

Graphene

Transport properties

GMR

Andreev reflection

ABSTRACT

This study delves into the transport properties of ferromagnetic-superconductor-ferromagnetic (FSF) junctions using graphene, where ferromagnetism and superconductivity are induced via proximity effect. The investigation focuses on the influence of ferromagnetic exchange energy and graphene energy bandgap. Fabricated on SiC and BN substrates, the graphene-based junctions treat charge carriers as massive relativistic particles. Utilizing a four-dimensional Dirac-Bogoliubov-de Gennes equation with tailored boundary conditions, the study calculates normal and Andreev reflection probabilities, alongside charge and spin conductances. Notably, oscillatory patterns in normal and Andreev reflection coefficients highlight the prevalence of Andreev reflection at lower energies, transitioning to normal reflection at higher energies. Conductivity trends with ferromagnetic exchange energy display a decline followed by an upturn beyond a critical point. The graphene energy bandgap notably influences Giant Magnetoresistance (GMR), with larger bandgaps yielding higher GMR magnitudes. These findings provide valuable insights into the intricate interplay among ferromagnetism, superconductivity, and graphene's electronic properties within FSF junctions. This understanding offers promising avenues for advancing graphene-based electronic and spintronic devices.

1. Introduction

Low-dimensional materials are those which are confined at least in one dimension. This sort of materials has unique properties that lead to the construction of new tools or improve the efficiency of some other structures [1-4]. Therefore, the acquisition of these materials is considered a revolution in physics and materials science.

Graphene, the first two-dimensional material and a unique carbon allotrope, consists of a single tightly packed layer of carbon atoms arranged in a hexagonal honeycomb lattice. In its primitive unit cell, there are precisely two atoms bonded together. This atomic structure gives graphene exceptional properties and makes it a promising candidate for various applications in fields such as electronics, photonics, and materials science [5,6].

Although graphene is basic building block for graphite but the characteristics of graphene are very different from those of graphite.

Regular graphene, fabricated on SiO₂, exhibits a semiconductor behavior with a zero-energy bandgap, stemming from the equivalence of its two carbon sublattices. In this configuration, carriers exhibit behavior akin to massless relativistic particles, referred to as massless Dirac fermions. They are characterized by a linear dispersion relation near the K point, given by $E(k) = \hbar k v_F$, where v_F (approximately 10⁶ m/s) represents the Fermi velocity, Figure 1(a). This unique band dispersion grants graphene exceptional electronic properties, notably its remarkably high charge carrier mobility, rendering it ideal for high-speed electronic devices [6,7]. Capitalizing on graphene's exceptional electrical, mechanical, and thermal attributes, graphene-based structures have found

* Corresponding author. Tel.: +98-918-3174181

E-mail address: h.karbaschi@gmail.com

Cite this article as:

Karbaschi, H., Rashedi, G., 2024. Electronic and spintronic transport in gapped graphene-based FG/SG/FG junctions. *Progress in Physics of Applied Materials*, 4(2), pp.115-121. DOI: [10.22075/PPAM.2024.34105.1100](https://doi.org/10.22075/PPAM.2024.34105.1100)

© 2024 The Author(s). Journal of Progress in Physics of Applied Materials published by Semnan University Press. This is an open access article under the CC-BY 4.0 license. (<https://creativecommons.org/licenses/by/4.0/>)

applications across diverse fields [3, 8-10].

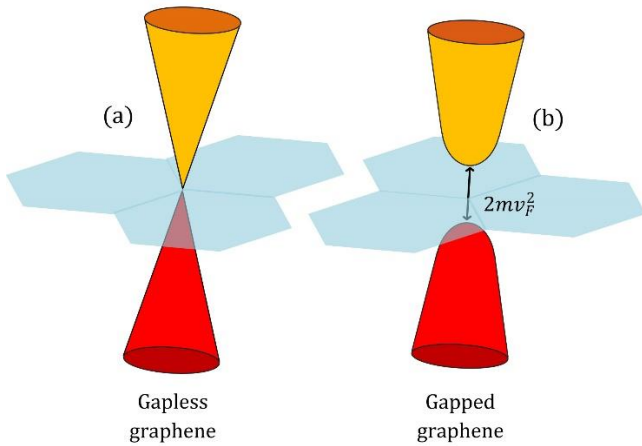


Fig. 1. Comparing quasiparticle energy spectra in (a) gapless and (b) gapped graphene systems.

Despite the exceptional carrier mobility of gapless graphene, its zero bandgap limits its application in electronic devices, unlike semiconductors such as silicon. Consequently, significant theoretical and experimental efforts have been undertaken to introduce a bandgap into graphene while preserving its remarkable transport properties [11-14]. One approach to opening a bandgap in graphene involves substrate-induced symmetry breaking [11]. The introduction of bandgaps in graphene, such as 50 meV on boron nitride (BN) substrates and 260 meV on silicon carbide (SiC) substrates, has been demonstrated experimentally [15]. Additional techniques for creating a bandgap into nanoribbons energy band structure involve doping [16], applying a magnetic field [17], inducing strain [18], and introducing structural defects [19]. In gapped graphene, carriers exhibit fermionic behavior akin to massive Dirac particles, Figure 1(b).

Recent research has validated the presence of proximity-induced ferromagnetism and superconductivity in graphene [20-23]. Consequently, designing based structures involving different phases has become highly attractive for studying various intriguing phenomena including supercurrent π -junction [24], spin-triplet correlation [25], Klein tunneling [26,27], spin conductance [28], Josephson junctions [29], and thermoelectricity [3,30].

Previously, a study was conducted on gapless graphene-based ferromagnetic-superconductor (FS) junctions [31]. To study the effect of the energy bandgap on the transport properties of such structures, we investigate the transport characteristics of pristine graphene-based ferromagnetic-superconductor-ferromagnetic (FSF) junctions, where the graphene is fabricated on substrates that open an energy bandgap in the energy band structure.

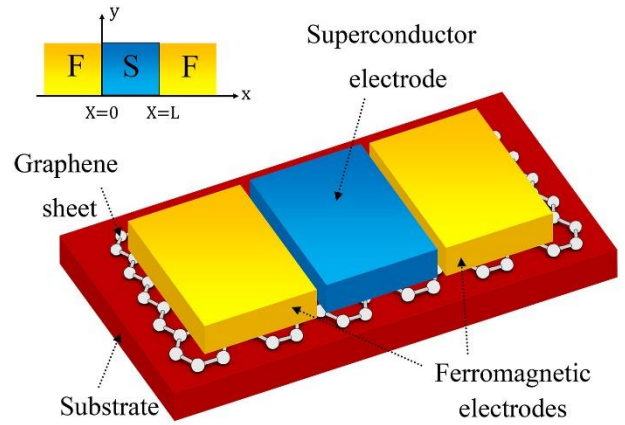


Fig. 2. Schematic sketch of a gapped FG/SG/FG junction.

In particular, we add a second ferromagnetic region to study the impact of parallel and antiparallel alignment of the ferromagnetic regions on the transport properties.

When analyzing a system containing a superconducting element, Andreev reflection stands out as a phenomenon significantly influencing its transport characteristics. Andreev reflection is a quantum mechanical process that occurs at the interface between a normal metal (or semiconductor) and a superconductor. When an electron from the normal metal with energy less than the superconducting energy gap is incident on the superconductor interface, it can be reflected as a hole within the superconductor. This process is accompanied by the creation of a Cooper pair (a bound state of two electrons with opposite spin and momentum) in the superconductor. Andreev reflection is a key mechanism in superconducting transport and plays a crucial role in phenomena such as the Josephson effect and proximity-induced superconductivity.

2. Calculation Method

We investigate pristine graphene-based ferromagnetic-superconductor-ferromagnetic junctions, where ferromagnetism and superconductivity are induced in graphene through the proximity effect, Figure 2. The generation of ferromagnetism in graphene via the proximity effect has been recently confirmed [20]. Additionally, the presence of intrinsic ferromagnetic correlations in graphene has been predicted [21].

The structures are assumed to be on three substrates: boron nitride (BN), silicon carbide (SiC), and a hypothetical substrate. In BN, we have $mv_F^2 = 0.0625E_F$, in SiC, $mv_F^2 = 0.325E_F$, and in the third substrate, $mv_F^2 = 0.5E_F$. For each structure, two cases are studied. The first involves parallel structures, where the magnetizations in both ferromagnetic parts are aligned upwards. The second case examines antiparallel structures, where the magnetization directions alternate between up and down. The structures are modeled in the xy -plane. Uniform thickness is assumed for all layers. We consider short and wide graphene nanoribbons where the width-to-length ratio (W/L) is much greater than 1. So, the microscopic edge details and chirality become negligible and can be ignored. This is because the bulk properties

dominate the behavior of the material, rendering the edge effects and specific chirality insignificant. By focusing on the bulk behavior and essential electronic properties, we capture the fundamental aspects relevant to the system's behavior while avoiding the complexities associated with edge effects and chirality [32,33].

To analyze the aforementioned systems, we need to solve the Dirac-Bogoliubov-de Gennes equation following the approach outlined in [22].

$$\begin{pmatrix} H_0 - \sigma h & \Delta \\ \Delta^* & -(H_0 - \bar{\sigma} h) \end{pmatrix} \begin{pmatrix} u_\sigma \\ v_{\bar{\sigma}} \end{pmatrix} = \varepsilon_\sigma \begin{pmatrix} u_\sigma \\ v_{\bar{\sigma}} \end{pmatrix}. \quad (1)$$

To solve the Dirac-Bogoliubov-de Gennes equation as described in [22], we use the Hamiltonian:

$$H_0 = -i\hbar v_F (\sigma_x \partial_x \pm \sigma_y \partial_y) - E_{FN} + \sigma_z m v_F^2, \quad (2)$$

Here, σ_x , σ_y , and σ_z are 2×2 Pauli matrices. ε_σ represents the energy relative to the Fermi level. \hbar and Δ denote the magnetization exchange energy and the order parameter in the ferromagnetic and superconducting regions, respectively. $\sigma = \pm 1$ corresponds to the up and down spin of the quasiparticle, and $\bar{\sigma} = -\sigma$. Both u_σ and $v_{\bar{\sigma}}$ have two components corresponding to the sublattices in the hexagonal lattice of graphene. Each spinor indeed comprises four components. Wave functions in each region are eigenstates of the Dirac-Bogoliubov-de Gennes equation. The electron-like wave function in the ferromagnetic region is expressed as:

$$\psi_{Fne\sigma}^\pm = \frac{e^{iqy \pm ik_{Fne\sigma} x}}{\sqrt{\cos \alpha_{n\sigma}}} \begin{pmatrix} 1 \\ \pm e^{\pm i \alpha_{n\sigma}} \\ 0 \\ 0 \end{pmatrix} \quad (3)$$

and for the hole-like part we have:

$$\psi_{Fnh\bar{\sigma}}^\pm = \frac{e^{iqy \pm ik_{Fnh\bar{\sigma}} x}}{\sqrt{\cos \alpha_{n\bar{\sigma}}}} \begin{pmatrix} 1 \\ 0 \\ 0 \\ \mp e^{\pm i \alpha_{n\bar{\sigma}}} \end{pmatrix} \quad (4)$$

In the ferromagnetic region, $\alpha_{n\sigma}$ represents the incidence angle with respect to the normal axis to the interface (the y -axis). Additionally, $k_{Fne\sigma}$ denotes the component of the electron-like wave vector perpendicular to the interface. In our calculations, $\mathbf{K} = k\hat{x} + q\hat{y}$ in the two-dimensional plane of graphene. They are respectively defined as follows:

$$\alpha_{n\sigma(\bar{\sigma})} = \sin^{-1} \left(\frac{\hbar v_F q}{\varepsilon + E_F + \sigma(\bar{\sigma})\hbar} \right) \quad (5)$$

$$k_{Fne\sigma(\bar{\sigma})} = \frac{\varepsilon + E_F + \sigma(\bar{\sigma})\hbar}{\hbar v_F} \cos \alpha_{1\sigma(\bar{\sigma})} \quad (6)$$

The solutions of the Dirac-Bogoliubov-de Gennes equation in the superconducting region take the following form:

$$\psi_{Se}^\pm = e^{(iqy \pm i(k_0 + i\chi)x)} \begin{pmatrix} e^{i\beta} \\ \pm e^{i(\beta \pm \gamma)} \\ 1 \\ \pm e^{i\gamma} \end{pmatrix} \quad (7)$$

$$\psi_{Sh}^\pm = e^{(iqy \mp i(k_0 - i\chi)x)} \begin{pmatrix} e^{-i\beta} \\ \mp e^{-i(\beta \mp \gamma)} \\ 1 \\ \mp e^{-i\gamma} \end{pmatrix} \quad (8)$$

$$\beta = \begin{pmatrix} \cos^{-1}(\varepsilon/\Delta_0) & \varepsilon \leq \Delta_0 \\ -i \cosh^{-1}(\varepsilon/\Delta_0) & \varepsilon > \Delta_0 \end{pmatrix} \quad (9)$$

$$k_0 = \sqrt{\left(\frac{\sqrt{(U_0 + E_F)^2 - (mv_F^2)^2}}{\hbar v_F} \right)^2 - q^2} \quad (10)$$

$$\chi = \left(\frac{\sqrt{(U_0 + E_F)^2 - (mv_F^2)^2}}{k_0 (\hbar v_F)^2} \right) \sin \beta \quad (11)$$

$$\gamma = \sin^{-1} \left(\frac{\hbar q v_F}{\sqrt{(U_0 + E_F)^2 - (mv_F^2)^2}} \right) \quad (12)$$

The determination of the appropriate transport coefficients involves imposing boundary conditions that ensure the matching of wave functions at all interfaces. These boundary conditions are outlined below:

$$\begin{aligned} \psi_{Fe}^\pm + r_N \psi_{Fe}^\mp + r_A \psi_{Fh}^\mp \\ = a \psi_{Se}^+ + b \psi_{Sh}^- + c \psi_{Se}^- + d \psi_{Sh}^+ \\ a \psi_{Se}^+ + b \psi_{Sh}^- + c \psi_{Se}^- + d \psi_{Sh}^+ \\ = t_{e\sigma} \psi_{Fe}^+ + t_{h\bar{\sigma}} \psi_{Fh}^- \end{aligned} \quad (13)$$

In the provided equations, $t_{e\sigma(\bar{\sigma})}$, r_N , and r_A represent the amplitudes of transmission for electron-like (hole-like) quasiparticles, normal reflection coefficients, and Andreev reflection coefficients, respectively. According to the Blonder-Tinkham-Klapwijk formula, the differential electronic conductance at zero temperature is derived as [22,31]:

$$G_q(\varepsilon) = \sum_{\sigma=\uparrow\downarrow} G_0 \int_0^{\pi/2} \cos \alpha_1 d\alpha_1 (1 + |r_A|^2 - |r_N|^2) \quad (14)$$

and the differential spintronic conductance at zero temperature is given by:

$$G_s(\varepsilon) = \sum_{\sigma=\uparrow\downarrow} \rho_\sigma G_0 \int_0^{\pi/2} \cos \alpha_1 d\alpha_1 (1 - |r_A|^2 - |r_N|^2) \quad (15)$$

In this equation, $G_0 = 2e^2/h N_\sigma(\varepsilon V)$ represents the spin-dependent normal conductance, where $\rho_\sigma = +1(-1)$ for $\sigma = \uparrow(\downarrow)$, and $N_\sigma(\varepsilon)$ denotes the density of states:

$$N_\sigma(\varepsilon) = \left(\sqrt{(\varepsilon + E_F + \sigma h)^2 - (mv_F^2)^2} \right) W / \pi \hbar v \quad (16)$$

Here, W represents the graphene-based FSF junction width (graphene strip). The assumption of zero temperature in the article simplifies the theoretical model and provides a clear baseline for understanding the fundamental mechanisms at play.

The upper integration limit is established by accounting for the conservation of the parallel component of the wave vector. An electron with spin σ , originating from the ferromagnetic (F) region, is allowed to enter the superconducting (S) region only if the incident angle α fulfills the condition $\alpha < \alpha_{c\alpha}$ [31].

$$\alpha_{c\sigma(\bar{\sigma})} = \sin^{-1} \left(\frac{\sqrt{(\varepsilon - E_F + \sigma(\bar{\sigma})h)^2 - (mv_F^2)^2}}{\sqrt{(\varepsilon + E_F + \sigma(\bar{\sigma})h)^2 - (mv_F^2)^2}} \right) \quad (17)$$

The computational analysis conducted in this article was performed using code written in Mathematica software. We chose not to discuss alternative methods like the tight-binding model for this study. By focusing on the bulk behavior and essential electronic properties, we capture the fundamental aspects relevant to the system's behavior while avoiding the complexities associated with edge effects and chirality. As a result, our computational approach, requiring fewer computations, will produce comparable results to more computationally intensive methods.

3. Numerical results and discussion

Figs. 3 and 4 illustrate the normal reflection (R_N) and Andreev reflection (R_A) coefficients in terms of ε/Δ for spin up and down quasiparticles in both parallel and antiparallel structures, considering three magnitudes of the graphene energy bandgap. The presence of spin-polarized states in the ferromagnetic regions leads to spin-dependent reflection processes, where the spin of the incident quasiparticle affects the probability and characteristics of the reflection.

For all cases, both normal and Andreev reflection coefficients exhibit oscillatory behavior with respect to quasiparticle excitation energy. This phenomenon arises from the coherent quantum interference of reflected quasiparticles from the second boundary with quasiparticles passing through the first boundary. For low-energy spin-up quasiparticles in the parallel structures, an increase in the graphene energy bandgap leads to a notable rise in the normal reflection coefficient. However, at high excitation energies, R_N becomes almost independent of the

energy bandgap size. Conversely, for spin-up quasiparticles in the antiparallel structure, there is an increasing trend in the normal reflection coefficient with the rise in the energy bandgap across all excitation energies.

It is evident that the normal reflection in spin-down quasiparticles is much less sensitive to changes in the energy bandgap size.

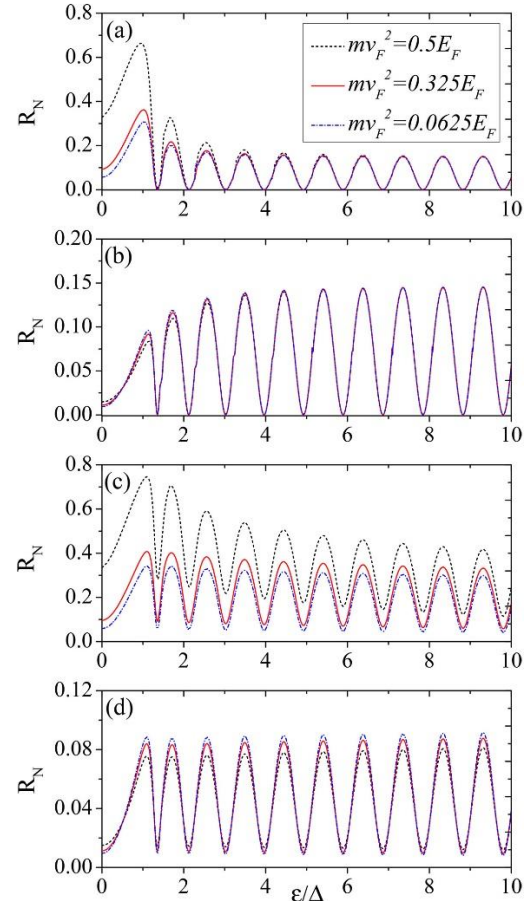


Fig. 3. Normal reflection coefficients in (a) spin up and parallel structure, (b) spin down and parallel structure, (c) spin up antiparallel structure, and (d) spin down antiparallel structure.

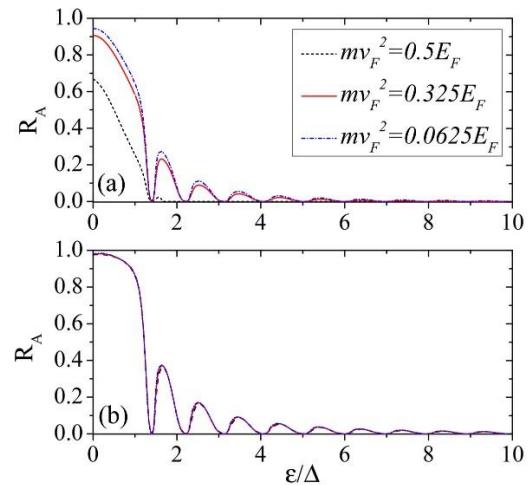


Fig. 4. Andreev reflection coefficients for (a) spin up, and (b) spin down quasiparticles.

An important observation from Figures 3 and 4 is that for low-energy quasiparticles, Andreev reflection is is

dominant, whereas for high-energy quasiparticles, normal reflection becomes decisive. Andreev reflection is significant at low energies because it involves the conversion of an incident electron into a hole, along with the creation of a Cooper pair in the superconductor. At low energies, the probability of Andreev reflection is higher compared to normal reflection because it is energetically favorable for the system to form a Cooper pair and conserve energy. Our calculation shows that Andreev reflection coefficient is independent of the magnetic direction in the second ferromagnetic part. In other words, Andreev reflection coefficient is independent of whether the structure is parallel or antiparallel.

Fig. 5 shows the normalized charge conductance (G_q) versus exchange energy of ferromagnetic layers for different graphene energy bandgaps. As we expected G_q of parallel cases are higher than G_q of antiparallel cases.

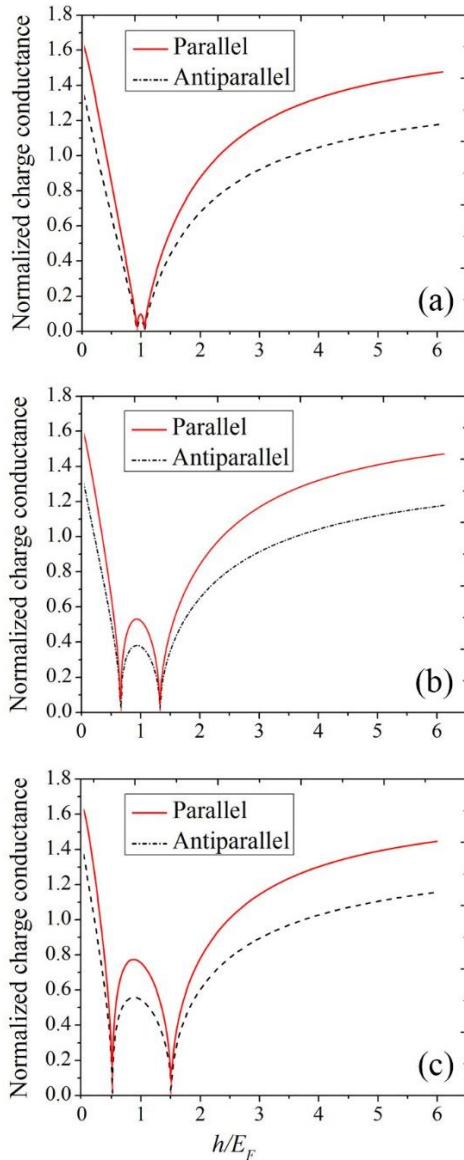


Fig. 5. (a), (b), and (c) Normalized charge conductance versus h/E_F of ferromagnets. The graphene energy bandgap is $0.0625E_F$, $0.325E_F$, and $0.5E_F$ respectively. Here, the thickness of graphene-based superconductive region is $kl=10$, $\Delta=0.01E_F$, and $\varepsilon=0.5\Delta$.

In all structures and within the range of $h < \varepsilon + E_F + mv_F^2$, conductivity decreases as ferromagnetic exchange energy increases. This occurs because in this range, both spin-up and spin-down subbands are of the same n-type. According to the equations 16 and 17, the increase in exchange energy results in a reduction in the density of states for spin-down quasiparticles (see Fig. 6) and a decrease in the number of conductivity modes for spin-up quasiparticles. Consequently, there is an increase in normal reflection and a decrease in Andreev reflection, ultimately leading to reduced conductivity.

In the regime where $h > \varepsilon + E_F + mv_F^2$, the Fermi level of spin-down electrons shifts into the valence band, imparting a p-n characteristic to the exchange field barrier. Under these conditions, an escalation in ferromagnetic exchange energy triggers a rise in Andreev reflection coupled with a decline in normal reflection, consequently enhancing conductivity. For large exchange energies, the barrier transforms into an almost perfect p-n barrier with a height of $2h$, facilitating the perfect transmission of chiral Dirac fermions between the two subbands. The increased Andreev conductance then reaches a maximum limit of 2.

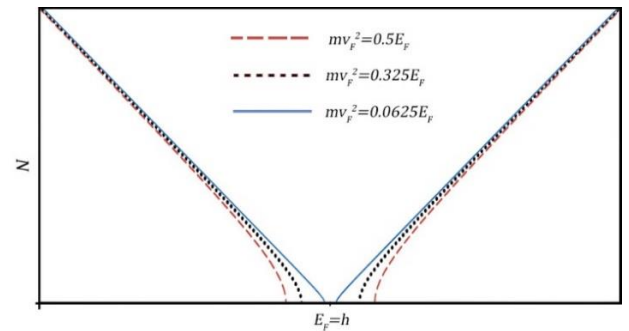


Fig. 6. Changes in the density of states as a function of exchange energy of the ferromagnetic region for three energy gaps.

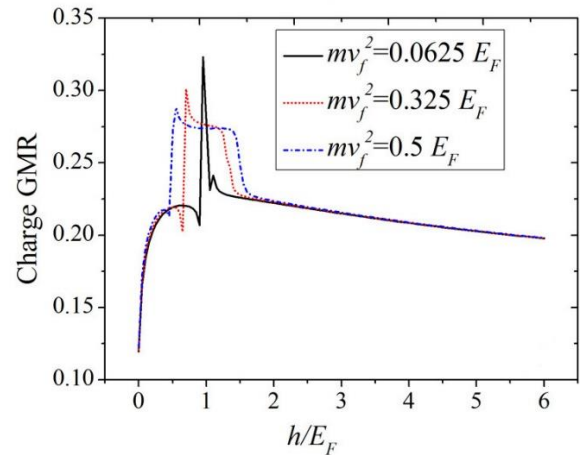


Fig. 7. Charge GMR in terms of h/E_F of ferromagnets for three magnitude of graphene energy bandgap.

In the transitional region between these two regimes, conductivity is affected by variations in the density of states and conductivity modes. Here, a peak in conductivity

occurs at $h=E_F$, and the height of this peak increases with the expansion of the energy bandgap. Also, In this energy range, which corresponds to the energy bandgap of graphene, the size of the Giant Magnetoresistance (GMR) is significantly larger than in other regions. Therefore, an increase in the energy bandgap leads to a larger GMR magnitude over a wider range, Figure 7.

Fig. 8 displays the normalized spin conductance as a function of the exchange energy of the ferromagnetic layers. The normalized spin conductance typically refers to a measure of how efficiently spin currents are transported through a material or device. It's often expressed as a ratio or a dimensionless quantity that normalizes the spin conductance to some reference value. Calculating the normalized spin conductance in parallel and antiparallel configurations is important for understanding how the relative alignment of magnetic moments affects spin transport properties.

Changes in spin conductance concerning ferromagnetic exchange energy are influenced by two factors. Firstly, an increase in ferromagnetic exchange energy induces spin-polarized currents and enhances spin transport. Secondly, an increase in h leads to reduced carrier transport in the range $h < \varepsilon + E_F + mv_F^2$ and increased carrier transport in the range $h > \varepsilon + E_F + mv_F^2$. Interestingly, spin conductance shows weak dependency on the size of the graphene energy gap. Regardless of the gap size, the spin transport curve remains similar in both small and large exchange energy regimes. Additionally, spin transport is consistently higher in parallel structures compared to antiparallel configurations.

4. Conclusion

In conclusion, our study on electronic and spintronic transport in gapped graphene-based FG/SG/FG junctions reveals several key findings. We observed that the behavior of spin-dependent normal and Andreev reflection, is strongly influenced by the graphene energy bandgap and the spin configuration of the junction. Particularly, Andreev reflection dominates at low energies due to its favorable energy conservation mechanism, while normal reflection becomes decisive at high energies. Furthermore, the conductivity of the system is affected by variations in the ferromagnetic exchange energy, exhibiting distinct behavior in different energy regimes. In the low exchange energy regime, conductivity decreases as the exchange energy increases due to changes in the density of states and conductivity modes.

Conversely, in the high exchange energy regime, conductivity is enhanced, especially when the exchange energy exceeds certain thresholds. We also found that the size of the graphene energy bandgap plays a crucial role in modulating the transport properties of the junction. In particular, the presence of the bandgap significantly affects

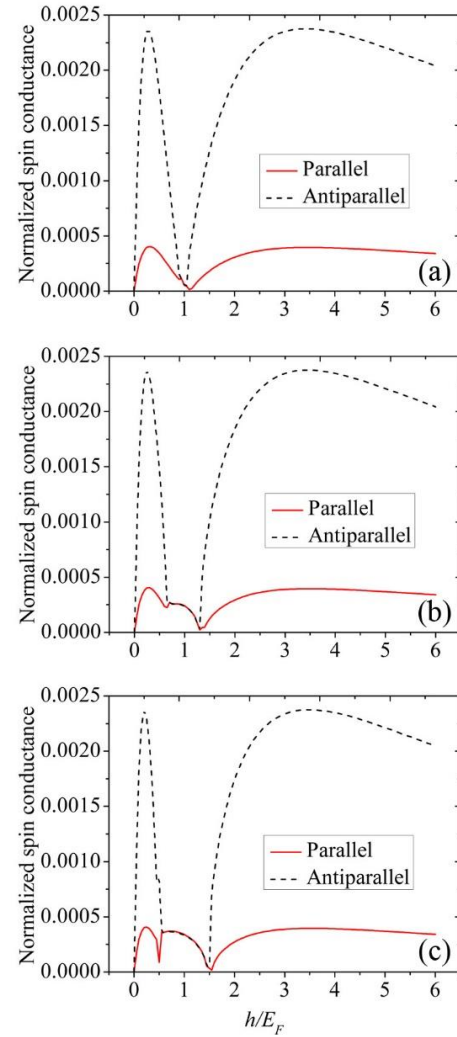


Fig. 8. (a), (b), and (c) Normalized spin conductance versus h/E_F of ferromagnets. The graphene energy bandgap is $0.0625E_F$, $0.325E_F$, and $0.5E_F$ respectively. Here, the thickness of graphene-based superconductive region is $kL=10$, $\Delta= 0.01E_F$, and $\varepsilon = 0.5\Delta$.

the magnitude of the Giant Magnetoresistance (GMR), with larger bandgaps resulting in larger GMR values. Overall, our results shed light on the intricate interplay between spin-dependent transport phenomena, exchange energy, and energy bandgap in graphene-based junctions. These findings provide valuable insights for the design and optimization of graphene-based spintronic devices with tailored transport characteristics.

Acknowledgements

Hossein Karbaschi would like to express his sincere gratitude to the Mahallat Institute of Higher Education for their unwavering support.

Conflicts of Interest

The author declares that there is no conflict of interest regarding the publication of this article.

References

- [1] Karbaschi, H., Lovén, J., Courteaut, K., Wacker, A. and Leijnse, M., 2016. Nonlinear thermoelectric efficiency of

- superlattice-structured nanowires. *Physical review. B*, 94(11).
- [2] Karbaschi, H., Rashedi, G. and Nouri, N., 2019. Thermoelectric cooling properties of quantum dot superlattice embedded nanowires. *Materials Research Express*, 6(9), p.095071.
- [3] Karbaschi, H. and Rashedi, G., 2019. Enhanced thermoelectric properties of graphene-based ferromagnetic-superconductor junctions, Andreev reflection effect. *Materials Research Express*, 6(6), p.065021.
- [4] Nouri, N., Rashedi, G. and Karbaschi, H., 2020. Analysis of electronic properties of Bismuth and Silicene antidot in the presence of strain using the four-orbital tight-binding method. *Physics Letters A*, [online] 384(17), p.126364.
- [5] Novoselov, K.S., Geim, A.K., Morozov, S.V., Jiang, D., Katsnelson, M.I., Grigorieva, I.V., Dubonos, S.V. and Firsov, A.A., 2005. Two-dimensional gas of massless Dirac fermions in graphene. *Nature*, [online] 438(7065), pp.197–200.
- [6] Geim, A.K. and Novoselov, K.S., 2007. The rise of graphene. *Nature Materials*, 6(3), pp.183–191.
- [7] Katsnelson, M.I., 2007. Graphene: carbon in two dimensions. *Materials Today*, 10(1-2), pp.20–27.
- [8] Aïssa, B., Memon, N.K., Ali, A. and Khraisheh, M.K., 2015. Recent Progress in the Growth and Applications of Graphene as a Smart Material: A Review. *Frontiers in Materials*, 2.
- [9] Asim, N., Badiei, M., Samsudin, N.A., Mohammad, M., Razali, H., Soltani, S. and Amin, N., 2022. Application of graphene-based materials in developing sustainable infrastructure: An overview. *Composites Part B: Engineering*, 245, p.110188.
- [10] Pang, J., Peng, S., Hou, C., Zhao, H., Fan, Y., Ye, C., Zhang, N., Wang, T., Cao, Y., Zhou, W., Sun, D., Wang, K., Rummeli, M.H., Liu, H. and Cuniberti, G., 2023. Applications of Graphene in Five Senses, Nervous System, and Artificial Muscles. *ACS Sensors*.
- [11] Zhou, S.Y., Gweon, G.-H., Fedorov, A.V., First, P.N., de Heer, W.A., Lee, D.-H., Guinea, F., Castro Neto, A.H. and Lanzara, A., 2007. Substrate-induced bandgap opening in epitaxial graphene. *Nature Materials*, 6(10), pp.770–775.
- [12] Cao, X., Shi, J., Zhang, M., Jiang, X., Zhong, H., Huang, P., Ding, Y. and Wu, M., 2016. Band Gap Opening of Graphene by Forming Heterojunctions with the 2D Carbonitrides Nitrogenated Holey Graphene, g-C₃N₄, and g-CN: Electric Field Effect. *The Journal of Physical Chemistry C*, 120(20), pp.11299–11305.
- [13] Nandee, R., Chowdhury, M.A., Shahid, A., Hossain, N. and Rana, M., 2022. Band gap formation of 2D material in graphene: Future prospect and challenges. *Results in Engineering*, 15, p.100474.
- [14] Wang, B. and Song, C., 2022. Graphene bandgap opening by constructing superlattices with BN or MoO₂ under pressure. *Journal of Physics: Conference Series*, 2331(1), pp.012001–012001.
- [15] Semenoff, G.W., V. Semenoff and Zhou, F., 2008. Domain Walls in Gapped Graphene. *Physical Review Letters*, 101(8).
- [16] Ajeel, F.N., Mohammed, M.H. and Khudhair, A.M., 2019. Energy bandgap engineering of graphene nanoribbon by doping phosphorous impurities to create nano-heterostructures: A DFT study. *Physica E: Low-dimensional Systems and Nanostructures*, 105, pp.105–115.
- [17] Do, T.-N., Shih, P.-H., Gumbs, G. and Huang, D., 2021. Influence of electric and magnetic fields and σ -edge bands on the electronic and optical spectra of graphene nanoribbons. *Physical review. B*, 103(11).
- [18] Zhao, T., Fan, Z.Q., Zhang, Z.H. and Zhou, R.L., 2019. Electronic structure, strain effects and transport property of armchair graphene nanoribbon with variously possible edge oxidation. *Journal of Physics D: Applied Physics*, 52(47), p.475301.
- [19] Kalami, R. and Ketabi, S. A., 2022. The electronic properties of armchair graphene nanoribbons defected by different shapes of quantum antidots. *Nanoscale* 9(1), pp.68–77.
- [20] Peres, R., M. A. N. Araújo and Bozi, D., 2004. Phase diagram and magnetic collective excitations of the Hubbard model for graphene sheets and layers. *Physical review. B, Condensed matter and materials physics*, 70(19).
- [21] Peres, N.M.R., Guinea, F. and Castro Neto, A.H. 2005. Coulomb interactions and ferromagnetism in pure and doped graphene. *Physical Review B*, 72(17).
- [22] C. W. J. Beenakker C. W. J., 2006. Specular Andreev Reflection in Graphene. *Physical review letters*, 97(6).
- [23] Wang, Z., Tang, C., Sachs, R., Barlas, Y. and Shi, J. 2015. Proximity-Induced Ferromagnetism in Graphene Revealed by the Anomalous Hall Effect. *Physical review letters*, 114(1).
- [24] Linder, J., Yokoyama, T., Huertas-Hernando, D. and Sudbø, A., 2008. Supercurrent switch in graphene Π junctions. *Physical review letters*, 100(18), p.187004.
- [25] Halterman, K., Valls, O.T. and Alidoust, M., 2013. Spin-Controlled Superconductivity and Tunable Triplet Correlations in Graphene Nanostructures. *Physical review letters*, 111(4).
- [26] Katsnelson, M.I., Novoselov, K.S. and Geim, A.K., 2006. Chiral tunnelling and the Klein paradox in graphene. *Nature Physics*, 2(9), pp.620–625.
- [27] Peres, N.M.R., 2009. The transport properties of graphene. *Journal of physics. Condensed matter*, 21(32), pp.323201–323201.
- [28] Beiranvand, R. and Hamzehpour, H., 2020. Switchable crossed spin conductance in a graphene-based junction: The role of spin-orbit coupling. *Scientific Reports*, 10(1).
- [29] Pellegrino, F.M.D., Falci, G. and Paladino, E., 2022. Effect of dilute impurities on short graphene Josephson junctions. *Communications Physics*, [online] 5(1), pp.1–10.
- [30] Bernazzani, L., Marchegiani, G., Giazotto, F., Roddaro, S. and Braggio, A., 2023. Bipolar Thermoelectricity in Bilayer-Graphene-Superconductor Tunnel Junctions. *Physical review applied*, 19(4).
- [31] Zareyan, M., Mohammadpour, H. and Moghaddam, A.G., 2008. Andreev-Klein reflection in graphene ferromagnet-superconductor junctions. *Physical Review B*, 78(19).
- [32] Katsnelson, M.I., 2006. Zitterbewegung, chirality, and minimal conductivity in graphene. *The European Physical Journal B - Condensed Matter and Complex Systems*, 51(2), 157 (2006).
- [33] Tworzydło, J., Trauzettel, B., Titov, M., Rycerz, A. and Beenakker, C.W., 2006. Sub-Poissonian shot noise in graphene. *Physical review letters*, 96(24), p.246802.